



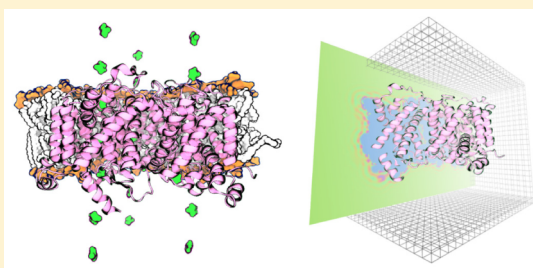
Potential of Mean Force Calculations of Solute Permeation Across UT-B and AQP1: A Comparison between Molecular Dynamics and 3D-RISM

Igor Ariz-Extreme and Jochen S. Hub*

Institute for Microbiology and Genetics, Georg-August-Universität, 37077 Göttingen, Germany

 Supporting Information

ABSTRACT: Membrane channels facilitate the efficient and selective flux of various solutes across biological membranes. A common approach to investigate the selectivity of a channel has been the calculation of potentials of mean force (PMFs) for solute permeation across the pore. PMFs have been frequently computed from molecular dynamics (MD) simulations, yet the three-dimensional reference interaction site model (3D-RISM) has been suggested as a computationally efficient alternative to MD. Whether the two methods yield comparable PMFs for solute permeation has remained unclear. In this study, we calculated potentials of mean force for water, ammonia, urea, molecular oxygen, and methanol across the urea transporter B (UT-B) and aquaporin-1 (AQP1), using 3D-RISM, as well as using MD simulations and umbrella sampling. To allow direct comparison between the PMFs from 3D-RISM and MD, we ensure that all PMFs refer to a well-defined reference area in the bulk or, equivalently, to a well-defined density of channels in the membrane. For PMFs of water permeation, we found reasonable agreement between the two methods, with differences of $\lesssim 3$ kJ mol⁻¹. In contrast, we found stark discrepancies for the PMFs for all other solutes. Additional calculations confirm that discrepancies between MD and 3D-RISM are not explained by the choice for the closure relation, the definition of the reaction coordinate (center of mass-based versus atomic site-based), details of the molecule force field, or fluctuations of the protein. Comparison of the PMFs suggests that 3D-RISM may underestimate effects from hydrophobic solute-channel interactions, thereby, for instance, missing the urea binding sites in UT-B. Furthermore, we speculate that the orientational averages inherent to 3D-RISM might lead to discrepancies in the narrow channel lumen. These findings suggest that current 3D-RISM solvers provide reasonable estimates for the PMF for water permeation, but that they are not suitable to study the selectivity of membrane channels with respect to uncharged nonwater solutes.



INTRODUCTION

Protein channels facilitate the selective flux of solutes across biological membranes. A popular quantity used to characterize the selectivity of channels is the potential of mean force (PMF) for solute permeation.^{1,2} The barriers and the minima along the PMF indicate the locations of the selectivity filters and solute binding sites, respectively. Since the height of the barriers is related to the permeability, PMFs help to quantify the selectivity of the channel with respect to different solutes.³ In previous studies, molecular dynamics (MD) simulations have been widely used to compute such PMFs for solute permeation across membrane channels, typically employing techniques such as umbrella sampling (US) or constrained MD.^{4–21} Despite common approximations, such as the neglect of polarization, as well as sampling limitations, MD simulations showed reasonable agreement with experimental permeability data, suggesting that the permeation process *in silico* resembles the experimental conditions.

In this work we compare two different approaches that have been used to compute PMFs across membrane channels, namely, the three-dimensional reference interaction site model (3D-RISM), and MD simulations using US. US is a well-

established method based on biased MD simulations, used to obtain sampling along the complete reaction coordinate.^{5,6,22–24} 3D-RISM is based on the statistical mechanics theory of liquids and aims to calculate three-dimensional site–site correlation functions of a solvent molecule around a complex solute.^{25–27} Compared to MD simulations, 3D-RISM calculations are computationally cheaper by orders of magnitude, thus in principle providing an attractive protocol to obtain the solvent distributions around proteins or inside protein channels.²⁸ 3D-RISM has been very popular in applications where water is the main solvent,^{29–35} including the detection of water molecules in protein cavities.^{36–38} Hence, 3D-RISM was used to predict the water density around and inside the water channel aquaporin-1 (AQP1), which can be readily translated into the PMF for water permeation.^{39–41}

To study the permeation of small nonwater solutes across protein channels, 3D-RISM must deal with solvent mixtures, since the distribution of both, water and the nonwater

Received: November 9, 2016

Revised: January 26, 2017

Published: January 27, 2017

permeating solute inside the channel, must be simultaneously computed. Such applications are challenging because the permeating solute competes with the abundant water for interactions with the protein in the channel's vestibule and, possibly, also inside the channel lumen. Hence, accurate calculations of the density of the permeating solute requires that the water–protein interactions are correctly balanced with respect to solute–protein interactions. In addition, if the permeating solute exposes a nonpolar surface, the calculations would require accurate treatment of the hydrophobic solute–protein interactions, which have remained challenging in the 3D-RISM context.^{34,42,43} Moreover, molecules often adopt well-defined orientations inside a narrow channel, whereas the RISM method takes averages over the solvent's orientational degrees of freedom. Whether the orientational average leads to artifacts in a narrow channel lumen has, to our knowledge, not been systematically addressed. 3D-RISM has been suggested to correctly describe solvent mixtures,⁴⁴ but applications have been mainly restricted to solvent mixtures of water and electrolyte,^{29,32,45–48} for which the above-mentioned challenges might be less critical. For instance, 3D-RISM was successfully used to identify ion binding sites in potassium channels.^{38,49–51} Whether 3D-RISM correctly describes the distribution of solvent mixtures of uncharged molecules inside protein channels, has remained unclear and triggered some lively discussions.^{41,52–54}

To test whether current 3D-RISM implementations provide a fast and general alternative to MD, we computed the PMFs of solute permeation across protein channels as derived by the two methods. The 3D-RISM calculations were conducted with the AmberTools software.⁴⁴ PMFs were computed for several solutes that strongly differ in hydrophobicity and size, thus allowing us to test the influence of such parameters on the agreement between MD and 3D-RISM. We considered the permeation across two prototypical membrane channels: the mammalian urea transporter UT-B and the water channel AQP1.

Urea transporters are a family of membrane proteins that mediate the flux of urea across the cell membrane.⁵⁵ UT-B is one of the most common urea transporters found in different bacterial and animal species, including mammals, where it is expressed in tissues such as kidney, brain, ear, testis, intestine, and bladder.⁵⁶ The structure and function of UT-B has been portrayed in several experimental and computational studies, which demonstrated also the efficient flux of water and ammonia (NH₃) across the channel.^{57–61}

Aquaporins are another widely expressed family of membrane channels facilitating water permeation across lipid membranes.⁶² They have been found in all domains of life.⁶³ AQP1 is one of the best studied aquaporins, with a well-characterized selectivity filter that is optimized for the permeation of small polar molecules but excludes larger molecules such as urea or glycerol.^{52,64–67}

THEORY AND METHODS

Theory. We first briefly review MD-based US and 3D-RISM. For a detailed introduction, we refer to a number of excellent reviews and textbooks.^{1,22,25,68}

Umbrella Sampling with MD Simulations. MD simulations integrate Newton's equations of motion, where the forces are given by an empirical force field.⁶⁹ Equilibrium MD simulations frequently suffer from poor sampling, because functionally relevant events, such as solute permeation across membrane

channels, often occur on time scales beyond the accessible simulation times. Hence, enhanced sampling methods such as US are required to study such rare events.

US has been widely used to compute PMFs from MD simulations.^{1,22} Originally proposed by Torrie and Valleau, this method applies a harmonic biasing potential to the system to ensure sampling along the whole reaction coordinate ξ .⁷⁰ Accordingly, the reaction coordinate is divided into multiple windows and, after the simulations have finished, the unbiased PMF $G_i(\xi)$ for each window i is recovered from the biased simulations following

$$G_i(\xi) = -(1/\beta) \ln P_i^b(\xi) - w_i(\xi) + F_i \quad (1)$$

Here $\beta = 1/k_B T$, where k_B is the Boltzmann constant and T the temperature, P_i^b denotes the biased distribution of window i , $w_i(\xi)$ is the biasing harmonic potential that restrained the system along ξ , and $F_i = -(1/\beta) \ln \langle \exp[-\beta w_i(\xi)] \rangle$. The brackets $\langle \cdot \rangle$ denote the ensemble average. P_i^b is extracted from a biased MD simulation. The PMF $G_i(\xi)$ of all windows and the constants F_i are typically computed with the weighted histogram analysis method (WHAM).⁷¹

3D-RISM. 3D-RISM is based on the integral equation theory of molecular liquids and provides a framework to compute solvent density distributions around a complex solute on a three-dimensional grid, as well as the thermodynamic properties such as hydration free energies.^{25,27} In this paragraph, we follow the nomenclature for “solute” and “solvent” as used in the 3D-RISM literature. Translated into the context of small-molecule permeation across a protein channel, the 3D-RISM “solute” refers to the protein only, whereas the 3D-RISM “solvent” describes both water and, if present, the additional permeating small molecules. In contrast, according to the terminology adopted in literature on protein channels, the term “solute” describes the permeating small molecule.

3D-RISM aims to solve the six-dimensional molecular Ornstein–Zernike (OZ) equations that relate the total correlation function $h(\mathbf{r}, \mathbf{r}')$ to the direct correlation function $c(\mathbf{r}, \mathbf{r}')$:

$$h_{uv}(1, 2) = c_{uv}(1, 2) + \int c_{uv}(1, 3) \rho_v h_{vv}(3, 2) d(3) \quad (2)$$

where the numbers in the parentheses represent the coordinates of particles in the liquid system, that is, the position \mathbf{R} and the orientation Ω . The symbol ρ denotes the particle number density, and the subscripts u and v indicate solute and solvent, respectively. One of the most common approaches to approximately solve eq 2 uses the site–site dielectrically consistent RISM equation (DRISM),^{72,73} which carries out the full orientational reduction of the molecular OZ equations. This results in the spatial correlation functions between the solvent atomic species sites, which are used subsequently to solve the 3D-RISM equation. Thus, 3D-RISM averages out the solvent molecular orientations, but it keeps the orientational description of the solute molecule:

$$h_{\alpha}^{uv}(\mathbf{r}) = \sum_{\gamma=1}^N \int_{\mathbb{R}^3} c_{\gamma}^{vu}(\mathbf{r} - \mathbf{r}') \chi_{\gamma\alpha}^{vv}(|\mathbf{r}'|) d\mathbf{r}' \quad (3)$$

where $\alpha = 1, \dots, N$, $\chi_{\gamma\alpha}(\mathbf{r})$ is the bulk solvent susceptibility function taken from DRISM, γ and α denote the indexes over the atomic species sites in a solvent molecule, and N is the number of atomic species sites in the solvent molecule.

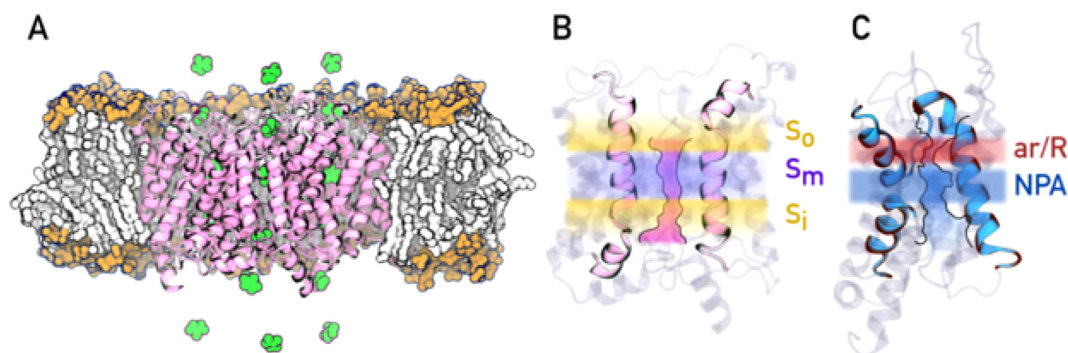


Figure 1. (A) Three-dimensional representation of a typical umbrella simulation system box. The lipid heads and tails are represented as orange and white spheres, respectively. The UT-B protein is shown in pink cartoon representation. The urea molecules placed along the reaction coordinate z (membrane normal) are depicted in green. (B) Schematic view of a UT-B monomer visualizing the pore topology as a pink area. The regions S_o , S_m , and S_i are highlighted by color. (C) Schematic view of the AQP1 monomer with the pore topology depicted as a blue area. The conserved asparagine-proline-alanine (NPA) region and aromatic/arginine (ar/R) constriction region are highlighted in color.

The solution to eq 2 includes multiple integrals that are difficult to solve except for some special cases. Therefore, to solve the OZ equations, both in DRISM and 3D-RISM, they have to be complemented by a closure relation. Several approximations have been developed for the closure relation such as the Percus–Yevick (PY), hypernetted-chain (HNC) or the mean-spherical (MSA) approximation.^{68,74,75} In this work, we used the Kovalenko-Hirata (KH) closure relation, as implemented in AMBER,⁴⁴ which combines the HNC closure for low-density regions with the MSA closure for high density regions.⁷⁶

$$h_{\alpha}^{uv}(\mathbf{r}) = \begin{cases} \exp[d_{\alpha}^{uv}(\mathbf{r})] - 1 & \text{for } d_{\alpha}^{uv}(\mathbf{r}) \leq 0 \\ d_{\alpha}^{uv}(\mathbf{r}) & \text{for } d_{\alpha}^{uv}(\mathbf{r}) > 0 \end{cases} \quad (4)$$

Here

$$d_{\alpha}^{uv}(\mathbf{r}) = -\beta u_{\alpha}^{uv}(\mathbf{r}) + h_{\alpha}^{uv}(\mathbf{r}) - c_{\alpha}^{uv}(\mathbf{r}) \quad (5)$$

Here, $u_{\alpha}^{uv}(\mathbf{r})$ denotes the interaction potential between the solute and solvent site α , given by the sum of the electrostatic and Lennard-Jones (LJ) potentials between the solvent site α and all solute atoms.

Computational Details. For this work, PMFs and simulation snapshots for AQP1 were taken from ref 52.

System Setup for US Simulations of UT-B. Initial coordinates of UT-B were taken from the Protein Data Bank (PDB code 4EZC).⁵⁷ Initial coordinates for the lipid membrane were taken from a 1 ns equilibrium simulation of a hydrated membrane of 328 (1-palmitoyl-2-oleoyl-*sn*-glycero-3-phosphocholine) POPC lipids. The protein was embedded in the membrane with the *g_membed* software,⁷⁷ and the simulation box was filled by explicit water and neutralized by one counterion. The final simulation system contained the UT-B trimer, 274 POPC molecules, 24989 TIP3P⁷⁸ water molecules, and 1 sodium ion.

Interactions of the protein atoms were described by the Amber ff99SB*-ILDN force field,⁷⁹ and lipid parameters were taken from Berger et al.^{80,81} The simulations were carried out with the GROMACS simulation software (version 4.6).⁸² Electrostatic interactions were calculated at every step with the particle-mesh Ewald method.⁸³ Short-range repulsive and attractive dispersion interactions were described by a LJ potential, with a cutoff at 1 nm. The geometry of water molecules was constrained with the SETTLE algorithm,⁸⁴ and

all other bond lengths were constrained with LINCS.⁸⁵ Hydrogen atoms of the protein were constructed as virtual sites, allowing a 4 fs time step.⁸⁶ The simulation temperature was controlled at 300 K using velocity rescaling ($\tau = 2.5$ ps),⁸⁷ and the pressure was kept at 1 bar with a semiisotropic Berendsen barostat ($\tau = 2$ ps).⁸⁸ The system was equilibrated for 150 ns before production. Figure 1 A shows a typical simulation box.

We computed PMFs for permeation across UT-B for the following solutes: TIP3P⁷⁸ water, ammonia (NH_3), urea, molecular oxygen (O_2), and methanol. Parameters for NH_3 were generated using *AmberTools15* from the AMBER molecular dynamics package,⁸⁹ with AM1-BCC charges,^{90,91} and the atoms were defined with the OPLS-AA force field.^{92,93} Urea parameters were taken from Duffy et al.⁹⁴ O_2 was modeled purely by LJ spheres, with parameters taken from the CHARMM22 force field.⁹⁵ For methanol, we used the GAFF parameters provided at <http://virtualchemistry.org/>.^{96,97}

US Simulation Details. The z -coordinate (membrane normal) was taken as reaction coordinate measured as the distance between the center-of-mass (COM) of the solute molecule to COM of the transmembrane backbone atoms of the protein. Starting frames for US were taken from a 150 ns equilibrium simulation. We placed 21 solute molecules per simulation (7 per monomer), allowing thus to collect 21 umbrella windows from each simulation. The solutes were separated by 1.5 nm in the z direction, and restrained by a harmonic umbrella potential with a force constant of 1000 kJ mol⁻¹ nm⁻². In addition, to ensure that the solutes adopt a well-defined membrane area outside the channel (in bulk), the solutes were restrained into cylinders aligned along the respective channel axis, as suggested by Allen et al.² In this work, the cylindrical restraint was implemented as a flat-bottomed quadratic potential, $V_{\text{cyl}}(r) = k_c(r - r_c)^2/2 \times H(r - r_c)$. Here, r denotes the distance from the cylinder axis that was aligned along the respective pore, $k_c = 1000$ kJ mol⁻¹ nm⁻² is the force constant, $r_c = 0.8$ nm is the cylinder radius, and H is the Heaviside step function. All the umbrella simulations were carried out using an in-house modified GROMACS simulation software (version 4.6) which implemented the flat-bottomed quadratic potential.

Adjacent umbrella windows were separated by 0.01 nm in simulations of water, urea, and NH_3 , thus requiring 150 simulation systems to cover the complete reaction coordinate. For O_2 and methanol, adjacent windows were separated by

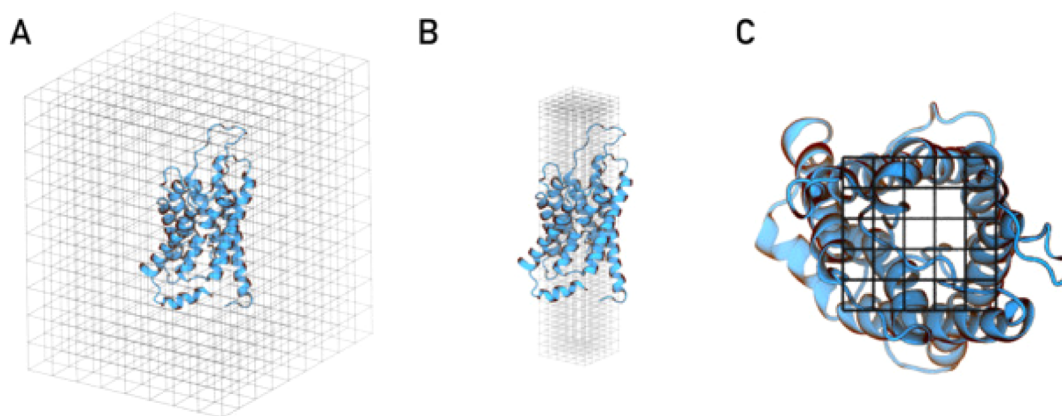


Figure 2. (A) Schematic view of AQP1 inside a 3D-RISM grid. (B) Reduced three-dimensional grid across the AQP1 pore. (C) *x* and *y* view of the aforementioned reduced area. The grids do not show the actual number of grid points.

0.025 nm, requiring 60 simulation systems. Umbrella simulations for urea were conducted for 10 ns, and all other umbrella simulations for 5 ns. The temperature was controlled using a stochastic dynamics integration scheme ($\tau = 0.5$ ps),⁹⁸ and the pressure was kept at 1 bar with the Parrinello-Rahman barostat ($\tau = 5$ ps).^{99,100} The box length in the *z* direction was kept fixed. We used a 2 fs time step during umbrella sampling. All other simulation parameters were identical to the equilibrium simulations.

PMF Construction after US. The first 2 ns of each trajectory were removed for equilibration for simulations with water, NH₃, O₂, and methanol and the first 4 ns for simulations with urea. In total, 11 970 umbrella histograms were collected from 3.6 μ s of simulation of the UT-B system. PMFs were calculated using a periodic implementation of WHAM.^{71,101} For each solute, histograms were collected from the three channels and subsequently combined into one PMF. Since we applied a cylindrical flat-bottomed potential, the PMFs refer to a channel density of one channel per cross-section area of the cylinder. Here, we corrected the PMFs such that they correspond to a channel density of one channel per membrane area occupied by a UT-B monomer. To this end, we used a trapezoidal correction between the entrance and exit regions of the pore as done previously,^{21,52} shifting the PMF by $k_B T \ln(A_{\text{mono}}/A_{\text{cyl}})$. Here, A_{mono} is the area occupied by a UT-B monomer and A_{cyl} is the effective cross-section area of the cylinder. The area of the cylinder was approximated as $A_{\text{cyl}} = \pi (r_c + 2\sigma_c)^2$, where $\sigma_c = (k_B T/k_c)^{1/2}$ is the width of the Gaussian-shaped distribution in the quadratic region of the flat-bottomed cylindrical potential. Indeed, the entropy of a uniform two-dimensional (2D) distribution in A_{cyl} approximately equals the entropy of a 2D distribution in a flat-bottomed quadratic potential, as derived in Appendix A. In addition, the PMFs were defined to zero in the bulk region. Statistical errors were calculated by bootstrapping complete histograms,¹⁰¹ yielding errors of ≤ 3 kJ mol⁻¹.

DRISM and 3D-RISM Calculation Details. Before the 3D-RISM calculations, we performed dielectrically consistent reference interaction site model (DRISM) calculations to obtain the bulk solvent susceptibility function $\chi_{\gamma\alpha}(\mathbf{r})$. We used the same solute parameters as in the MD simulations except for the water and O₂ molecules. Water parameters were described by the TIP3P RISM model provided with the AMBER software,⁴⁴ which, in contrast to the default TIP3P, assumes LJ interactions for the hydrogen atoms. For O₂, we used the LJ

parameters from the CHARMM22 force field,⁹⁵ and the partial charges were set to zero.

DRISM calculations were carried out using the `rism1d` program of the AmberTools 14 molecular modeling package,^{44,89} at a temperature of 300 K and a dielectric constant of $\epsilon = 78.497$. Following the RISM implementation of the AmberTools,⁴⁴ no corrective bridge functions were applied,^{102–104} and no orientational correlation were included. We used a grid of 32,768 points with a grid spacing of 0.025 Å. All solvent mixtures were defined using a water concentration of 55.5 M and a solute concentration of 0.5 M. We used the MDIIS accelerated numerical solver¹⁰⁵ with 20 vectors, a step size of 0.3 and a residual tolerance of $1 \cdot 10^{-12}$, with the Kovalenko-Hirata closure relation.

For 3D-RISM calculations, we used the crystal structures of UT-B and AQP1 (PDB ID codes 4EZC and 1J4N).^{57,65} The interactions of the protein atoms were described by the Amber ff99SB*-ILDN force field.⁷⁹ To test the influence of protein fluctuations on PMFs, we also took 100 UT-B structures and 100 AQP1 structures from an equilibration simulation, and 100 UT-B structures from an umbrella simulation in which urea is bound to UT-B.

We carried out 3D-RISM calculations using the `rism3d.snglpnt` program in the AmberTools 14 molecular modeling package,^{44,89} at a temperature of 300 K. For UT-B, we used the trimer structure and a grid of $240 \times 224 \times 180$ points in a box of size $120 \times 112 \times 90$ Å³. For AQP1, we used the monomer structure, in a grid of $160 \times 140 \times 192$ points and a box of $80 \times 70 \times 96$ Å³. Figure 2 A shows a typical 3D-RISM grid around AQP1. In both systems, the distance of grid boundary to the protein was at least 15 Å. The MDIIS solution converged with a residual error between 10^{-5} and $2 \cdot 10^{-3}$ using 5 vectors, a step size of 0.7 and the Kovalenko–Hirata closure. To test the influence of other closures, we also converged the 3D-RISM solutions with the chained PSE₁/PSE₂ and PSE₁/PSE₂/PSE₃ as suggested by Giambaşu et al.¹⁰⁶

PMF Construction after 3D-RISM. We took the membrane normal *z* as the reaction coordinate, where $z = 0$ was defined either as the COM of the transmembrane region of UT-B or as the COM of the NPA motif of AQP1. The PMFs were computed from 3D-RISM results using the three-dimensional density $g_\alpha(\mathbf{r}) = h_\alpha(\mathbf{r}) + 1$, where α is the atomic species site of the permeating molecule. The α sites considered for each solute were the following: oxygen atom for water, nitrogen atom for NH₃, carbon atom for urea and methanol, and oxygen atom for

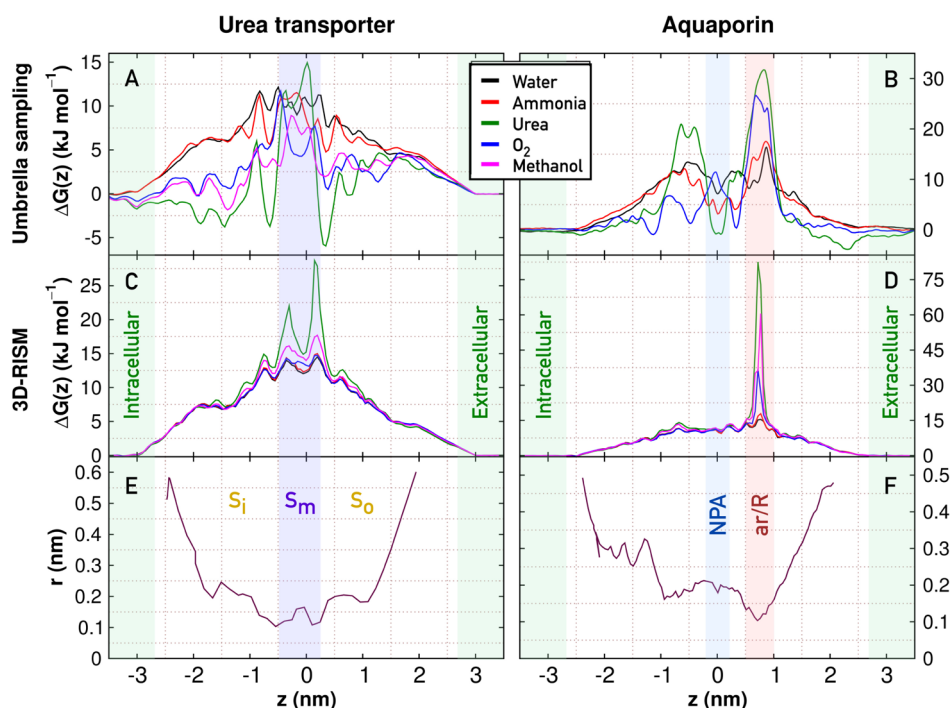


Figure 3. (A/B) PMFs $\Delta G(z)$ for solute permeation along the channel coordinate z from US simulations, and (C/D) from 3D-RISM based on the respective crystal structure. PMFs are shown for the urea transporter UT-B (A/C) and AQP1 (B/D). Different solutes are represented by different colors (see legend). (E/F) Radius of the channels computed with PROPORES.¹⁰⁷ $z = 0$ corresponds to the COM of the transmembrane residues in UT-B, and to the COM of the NPA motif in AQP1.

O₂. (Note that the number of atoms in the solute molecule is irrelevant because the density is normalized to unity in the bulk.) Hence, we computed the 3D-RISM PMFs from the density of solvent sites that are close to the center of mass of the respective solvent molecule. This is important to allow direct comparison with the PMFs from umbrella sampling, for which the molecule's center of mass was used to define the reaction coordinate. However, we also computed the PMFs from 3D-RISM based on the density of different solvent sites, and we found that the choice of the solvent site has only a minor effect on the PMFs (see the Discussion).

The three-dimensional (3D) density $g_\alpha(\mathbf{r})$ was reduced to the one-dimensional (1D) density distribution function $g_\alpha(z)$ by integrating out the x and y coordinates:

$$g_\alpha(z) = \int_{A_g(z)} g_\alpha(\mathbf{r}) dx dy \quad (6)$$

In the bulk water and in the vestibule regions, the integration area $A_g(z)$ was taken as a square with an area of $(1.6 \text{ nm})^2$, which is smaller than the monomer area in both proteins. A_g was centered along the respective monomer center, as visualized in Figure 2, parts B and C. In the pore region $|z| < 1 \text{ nm}$, $A_g(z)$ was taken as a square centered along the channel center, with a side length $2(r_c(z) + 3 \text{ \AA})$, where $r_c(z)$ is the channel radius. Here, the channel center and radii were computed with PROPORES.¹⁰⁷ Hence, the integration area A_g was large enough to account for the entropic effect from the tightening of the pore with respect to the bulk, and small enough to exclude the lipid membrane region. This procedure was required because the 3D-RISM calculations were carried out with the protein in vacuum and not embedded in a lipid membrane, thus generating unphysical solvent density in the lipid membrane region. In addition, restricting the integration

to a smaller square in the pore region excludes solvent droplets inside the protein matrix that are separated from the channel and do not contribute to permeation.

To average over multiple monomers or structures from simulation frames, we first averaged the density before computing the PMF:

$$\Delta G_\alpha(z) = -k_B T \ln \frac{\langle g_\alpha(z) \rangle_c}{g_\alpha(z_{\text{bulk}})} \quad (7)$$

where $\langle \cdot \rangle_c$ denotes the average over monomers and/or simulation frames, and z_{bulk} is a z -position in bulk water. Note that the factor $1/g_\alpha(z_{\text{bulk}})$ does not change the shape of the PMF but merely defines the PMF to zero in the bulk. To facilitate the direct comparison between the PMFs obtained with 3D-RISM and the ones obtained with US MD simulations, we used the same trapezoidal correction described above, using a correction of 4.21 kJ mol^{-1} and 3.47 kJ mol^{-1} for UT-B and AQP1, respectively, given by the bulk area of $A_g(z)$ and the monomer area. Hence, the 3D-RISM PMFs shown below correspond to a channel density of one channel per cross section area of the monomer.

IC₅₀ Estimate. Following the calculation in ref 19, the IC₅₀ value of a solute bound to one of the binding sites of the channel is given by $\text{IC}_{50} = (A_{\text{mono}} \int_{\text{ch}} \exp[-\beta \Delta G(z)] dz)^{-1}$, where the integral is taken across the channel. The symbol $\Delta G(z)$ denotes the PMF that is defined to zero in bulk water.

Translating Water PMF into Water Occupancy Inside the Channel. Because our PMFs correspond to a well-defined reference area in the bulk, they can be translated into the equilibrium one-dimensional (1D) solute density along the channel coordinate z at a given solute concentration in the bulk. Below, we use this fact to translate the PMFs of water permeation into the equilibrium water occupancy of the

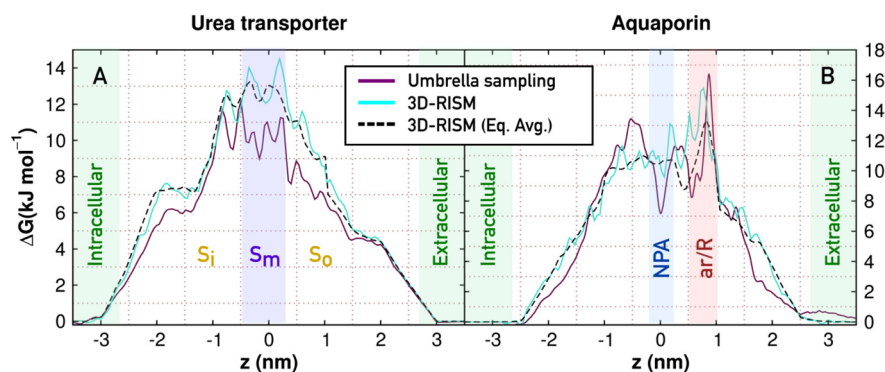


Figure 4. Water PMFs $\Delta G(z)$ calculated with US simulations (brown), 3D-RISM with the crystal structure (turquoise) and 3D-RISM after averaging over 100 equilibration simulation snapshots (black-dashed) for UT-B channel (A) and AQP1 (B). The S_i , S_m , and S_o regions are highlighted for UT-B, as well as the NPA motif and the ar/R region for AQP1.

channels. In bulk, the water 1D density $(\Delta N_w/\Delta z)_{\text{bulk}}$ is given by (i) the reference area of the PMF, for which we chose the cross section area of one monomer A_{mono} (10.3 nm² and 13.9 nm² for AQP1 and UT-B, respectively), and (ii) the number density of water (33.4 nm⁻³). Hence, we obtain for $(\Delta N_w/\Delta z)_{\text{bulk}}$ the values 344.3 nm⁻¹ and 463.6 nm⁻¹ for AQP1 and UT-B, respectively. Since we defined the PMF to zero in the bulk, the 1D water density along the pore is $(\Delta N_w/\Delta z)(z) = (\Delta N_w/\Delta z)_{\text{bulk}} \exp[-\beta \Delta G(z)]$. Integrating $(\Delta N_w/\Delta z)(z)$ across the channel lumen yields the equilibrium water occupancy.

RESULTS

PMFs from Umbrella Sampling. Figures 3 A and B present the PMFs $\Delta G(z)$ for the permeation of water, NH₃, urea, O₂, and methanol (see legend) across UT-B and AQP1, respectively. We computed the PMFs for UT-B as described in the Methods, and the PMFs for AQP1 were taken from ref 52.

For UT-B, Figure 3 A shows that all the free energy barriers ΔG^\ddagger are ≤ 15 kJ mol⁻¹, suggesting that UT-B represents a rather unspecific channel for small neutral solutes. Overall, these PMF are in agreement with previous computational studies.^{57,59,60} The PMFs for polar solutes such as water, NH₃, and urea, exhibit a higher free energy at $z \approx 0$ as compared to the more hydrophobic solutes O₂ and methanol, underlining the hydrophobic character of the S_m region next to the residues T172 and T334 (blue bar in Figure 3, parts A, C, and E).

The PMF for urea, the physiological substrate of the channel, exhibits several minima indicative of urea binding sites, resembling the PMF reported by Levin *et al.* for the channel lumen. The shoulder at $z = -1$ nm (S_i region) and the minimum at $z = 0.4$ nm (S_o region) correspond to the selenourea binding sites in the 4EZD crystal structure. At the pronounced minimum at $z = -0.6$ nm, no selenourea was found in the crystal structure, possibly because of different packing to the protein of selenourea as compared to urea. Since our PMFs expand into the bulk, they allow us to compute the urea concentration at the binding sites as compared to bulk water or, equivalently, an IC₅₀ concentration for urea binding (Methods). We obtain an IC₅₀ of 20 mM, suggesting that a significant fraction of urea channels in the kidney are occupied by urea at physiological urea concentrations.¹⁰⁸

The PMFs for water and NH₃ exhibit barriers of only ~ 12 kJ mol⁻¹, which reflect purely the entropic cost for entering the narrow lumen from the bulk water (Figure 3 A, black and red curves, and Figure 3 E). Hence, our PMFs are in line with the

notion of UB-T as an efficient channel for both water and NH₃, as suggested previously.⁵⁹ Likewise, PMFs for methanol and O₂ exhibit only low barriers. However, the PMFs of the five solutes clearly differ, reflecting different hydrophobicities and shapes of the solutes.

The AQP1 PMFs calculated with US simulations shown in Figure 3B have been discussed in ref 52. In short, the PMFs demonstrate that the selectivity of the channel is determined at the aromatic/arginine (ar/R) constriction region (Figure 3B, red bar), which allows the permeation of small polar solutes, but excludes hydrophobic and large solutes. The ar/R region constitutes the narrowest part of the pore, thereby excluding large solutes such as urea via steric effects (Figure 3 B). Small apolar solutes, such as O₂, are excluded because their permeation would require breaking of strong hydrogen bonds between water and the conserved arginine in the ar/R site.¹⁸ Because the interactions between apolar solutes and arginine are weaker than water-arginine interactions, apolar solutes feel a free energy barrier at the ar/R site. Hence, the modulations in the PMFs reflect steric, hydrophobic, as well as effects from polar interactions such as hydrogen bonds.

PMFs from 3D-RISM. In the following, we compare the PMFs calculated with 3D-RISM for water, NH₃, urea, O₂, and methanol across UT-B and AQP1 to the PMFs calculated with US simulations. The PMFs from 3D-RISM were computed from the three-dimensional solvent density following the procedure outlined above. In particular, to allow direct comparison to the PMFs from US, the PMFs from 3D-RISM were normalized with respect to the monomer cross section area using a trapezoidal correction between the entrance and exit regions of the pores (see Methods and Appendix A).

Figure 4 presents the water PMFs across UT-B (Figure 4A) and AQP1 (Figure 4B) calculated with 3D-RISM and the respective crystal structure (turquoise curve), as well as from US simulations (brown curves). We found reasonable agreement between the two methods, with differences of $\lesssim 4$ kJ mol⁻¹. For UT-B, 3D-RISM yields slightly higher PMFs as compared to US, reflecting lower water density inside the pore. To test if 3D-RISM was biased by the static crystal structure, we also computed PMFs with 3D-RISM as an average over 100 structures taken from equilibrium MD simulations (Figure 4, dashed curves). For UT-B, taking such equilibrium fluctuations of the channel into account, we found even closer agreement between 3D-RISM and US, with differences of $\lesssim 2$ kJ mol⁻¹. However, a slightly lower water density suggested by 3D-RISM as compared to US remains.

An intuitive quantitative comparison between MD and 3D-RISM is given by the average number of water molecules inside the narrowest channel lumen, which can be computed from the PMF (Methods). The results are summarized in Table 1. The

Table 1. Average Water Occupancy in the Narrowest Region of the Channel Lumen of UT-B ($-0.8 \text{ nm} < z < 0.3 \text{ nm}$) and AQP1 ($-1 \text{ nm} < z < 1 \text{ nm}$) As Computed from the PMFs^a

	3D-RISM (cryst.)	3D-RISM (av.)	MD
UT-B	3.1	3.2	7.8
AQP1	8.3	10.4	10.4 (7.7)

^a3D-RISM results computed using only the crystal structure or from an average over 100 MD simulations frames. MD result in brackets was computed by counting water molecules during an equilibrium simulation, taken from ref 52.

water occupancy during MD simulations suggests that the channels are fully filled by water, possibly as a zigzag-shaped water file. This is consistent with MD simulations reported by other authors.^{16,17,109} 3D-RISM calculations yield slightly reduced water densities in the UT-B lumen as compared to the MD result, and 3D-RISM quantitatively agrees with MD for AQP1. Noting that the 3D-RISM calculations were orders of magnitude faster than MD, the overall agreement is remarkable.

However, this agreement between the two methods for water is not found for the nonwater solutes (Figure 3, parts C and D). In contrast to the PMFs computed from US simulations, which highlight stark differences between different solutes (Figure 3, parts A and B), we found that the PMFs computed with 3D-RISM closely resemble each other. Notably, the PMFs for water, NH₃, urea, O₂, and methanol are virtually identical except for the S_m region in UT-B and the ar/R constriction site in AQP1. In the 3D-RISM calculations, the polarity of the solute seems to have only little influence on the PMFs, but the PMFs seem to be strongly dominated by the size of the solute, leading to increasing barriers with increasing solute size. Consequently, the urea binding sites in UT-B found in our and other work⁵⁷ from US (Figure 3A) are absent in the PMF computed with 3D-RISM (Figure 3A,C, green curves). At the ar/R site of AQP1, the 3D-RISM PMFs for urea, O₂, and methanol exhibit sharp barriers, higher than in the PMFs from US.

To test again if 3D-RISM was biased by the static crystal structure of UT-B and AQP1, we took 100 snapshots, each from equilibrium MD simulations of UT-B and AQP1, and we computed PMFs of urea with 3D-RISM for each single structure (Figure 5 A/C, gray). In addition, we averaged the density from all 100 snapshots and translated the averaged density into a mean PMF (Figure 5 A,C, black; see also Methods). The maximum difference between a PMF from a single snapshot and the respective mean PMF is about ~ 120 and $\sim 25 \text{ kJ mol}^{-1}$ for UT-B and AQP1, respectively. This suggests that protein fluctuations may have a strong effect on 3D-RISM results at tight constriction sites. Notably, the mean PMF for urea permeation across AQP1 exhibits a barrier of only 17 kJ mol^{-1} , which would imply that AQP1 conducts urea, contrasting experimental findings.⁶⁷ The strong influence of protein fluctuations on the 3D-RISM PMFs suggests that the adaptation of the UT-B channel lumen to a bound urea might be crucial for 3D-RISM results.

To test if the urea PMFs calculated with 3D-RISM did not reflect the urea binding sites in UT-B due to the lack of the

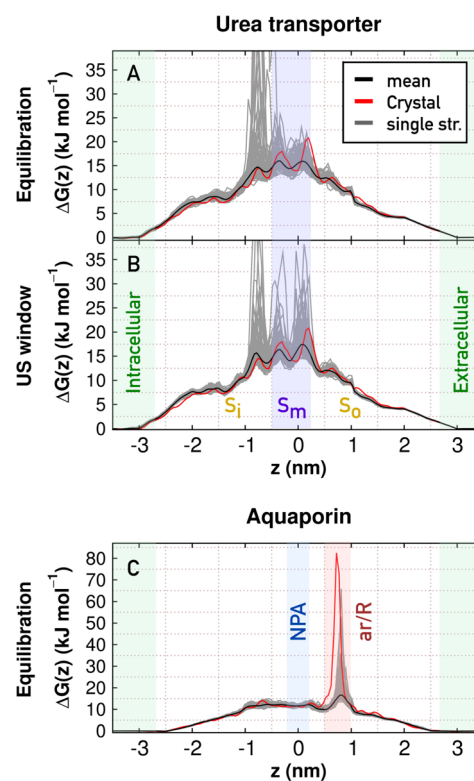


Figure 5. Urea PMFs $\Delta G(z)$ calculated with 3D-RISM across UT-B channel (A/B) and AQP1 (C) over 100 structures taken either from an equilibrium simulation or the umbrella window where urea is in the binding site of UT-B (gray), mean PMF of the respective 100 structures (black) and the PMF obtained from the crystal structure (red). The S_i, S_m, and S_o regions are highlighted for UT-B, as well as the NPA motif and the ar/R region for AQP1. The peaks were removed for clarity.

proper channel lumen structure, we took 100 snapshots from an umbrella window simulation in which urea is bound to UT-B at $z = 0.3 \text{ nm}$, and we computed the 3D-RISM PMF for each structure (Figure 5B, gray). None of these urea PMFs exhibits a minimum at $z = 0.3 \text{ nm}$, suggesting that, even when the channel lumen structure is adapted to urea, 3D-RISM did not identify the binding site.

We further tested if the closure relations used for DRISM or 3D-RISM influence the PMFs (Tables S1 and S2). Figure 6 presents PMFs for water, NH₃, urea, O₂, and methanol computed with 3D-RISM across UT-B and AQP1, either computed with the KH closure (black lines) or using chained PSE₁/PSE₂/PSE₃ closures (red lines). PMFs computed with additional closures are shown Figure S1. We found that, for most cases, changing the closure relation has only a small effect on the PMFs. Notable exceptions are the PMF for water and ammonia permeation across AQP1. In the ar/R region of AQP1, the water and NH₃ PMFs show differences of ~ 10 and $\sim 15 \text{ kJ mol}^{-1}$, respectively, suggesting that 3D-RISM with the PSE_n closure relations underestimates the water density in the narrow ar/R region (Figure 6, top right).

DISCUSSION

We have presented a systematic comparison between 3D-RISM, as implemented in the AmberTools software, and MD simulations, with a focus on PMF calculations for solute permeation across membrane channels. In this study, our aim

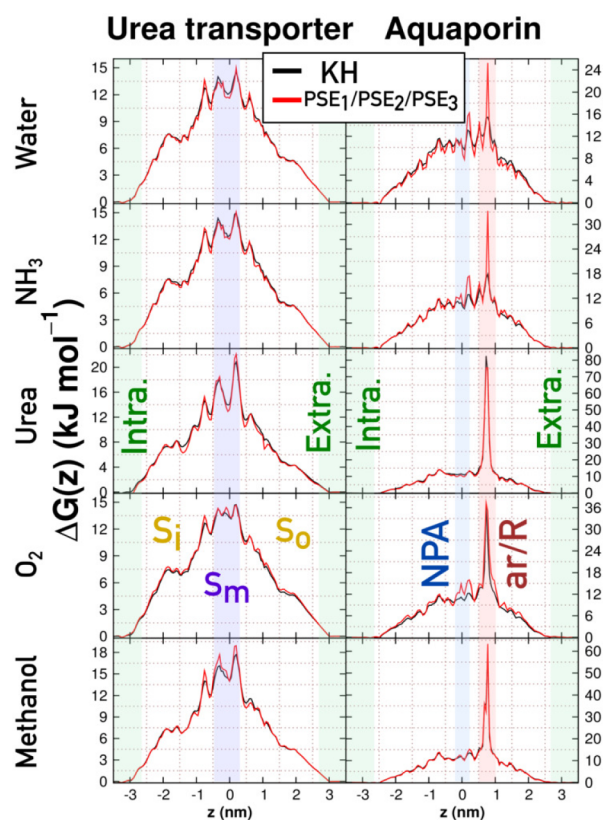


Figure 6. Water, NH_3 , urea, O_2 , and methanol PMFs $\Delta G(z)$ calculated with 3D-RISM across UT-B channel (left) and AQP1 (right) using the KH closure and the chained PSE-1, PSE-2 and PSE-3 closures. The S_i , S_m , and S_o regions are highlighted for UT-B, as well as the NPA motif and the ar/R region for AQP1. For most PMFs, we find that the closure relation has only a small effect on the PMFs.

was not to exactly match the theoretical frameworks of MD and 3D-RISM, for instance by applying mathematically identical Hamiltonians during all calculations. Instead, we mainly compared MD and 3D-RISM using setups as they are typically used by the communities, which, we believe, is a useful approach in the search for efficient computational methods. However, we also stress that we took extensive efforts to exclude that the main findings of this study depend on such common differences between MD and 3D-RISM, involving protein fluctuations, the definition of the reaction coordinate, and details of the force field. We found that these differences do not affect the main conclusions of this work.

For water as permeating solute, we found reasonable agreement between MD simulations and 3D-RISM. This agreement complements several successful applications of 3D-RISM for accurate calculations of water densities in biological systems.^{28,36–38,110} Notably, MD-based permeability calculations for aquaporins found reasonable agreement with experimental data in previous studies, suggesting that the 3D-RISM water density likewise resembles the experimental conditions in such channels (ref 111 and references therein). The small deviations between MD and 3D-RISM could be partly attributed to the lack of protein fluctuations, when the 3D-RISM calculations were based on the crystal structure only. Remaining differences between the water PMFs may be explained by the slightly different water models used for MD and 3D-RISM,⁴⁴ sampling limitations in the MD simulations, as

well as by the orientational averaging underlying the RISM approach.

For nonwater solutes, however, we observed large discrepancies between the PMFs from MD and 3D-RISM. The PMFs from MD strongly depend on the polarity, size, and shape of the solute, reflecting modulations in protein-solute interactions, hydrophobic effects, as well as competition between the solute with the abundant water for forming contacts with the protein. In particular, in apolar regions of the channel, the PMFs are lower for solutes that form partly apolar contacts with the protein (O_2 , methanol, and urea), thereby replacing unfavorable water-protein contacts. The PMFs from MD reasonably agree with results from previous MD studies.^{57,59–61,112} In contrast to the PMFs from MD simulations, the PMFs calculated with 3D-RISM appear too similar in major parts of the channel. In both channels, the variations in the PMFs between different solutes seem to reflect mainly the size of the solute, but 3D-RISM seems to miss modulations due to different polarities of the solutes. These findings may be explained by previous observations that 3D-RISM faces limitations at hydrophobic surfaces⁴³ and, possibly, due to the lack of orientation correlations.⁴⁴

The lack of urea binding sites in the PMFs calculated with 3D-RISM across UT-B (Figure 3C, green curve, and Figure 5A,B) deserves more explanation. As shown in Figure 7A,B the binding site in the S_o region is optimized for the asymmetric urea molecule. Here, urea may act as a hydrogen bond acceptor to T334 and as a hydrogen bond donor to the backbone oxygen atoms of I228 and Q227 (Figure 7A). In addition, the two planar and less polar surfaces of urea may form favorable contacts with the hydrophobic residues F283, L123, L127, and L287 (Figure 7B). Hence, by the combination of polar and apolar interactions, urea is locked into a well-defined orientation and energetically stabilized, leading to the pronounced minimum of approximately -5 kJ mol^{-1} in the PMF (Figure 3A, green curve). In contrast, the density of the urea carbon taken from 3D-RISM does not exhibit any binding site, but instead shows even reduced density (Figure 7C). These findings may indicate that the loss of information due to the orientational average of solvent molecules, as conducted by DRISM,^{25,44,68} could affect the final 3D density distribution of solvent molecules inside a protein channel, where the orientation of the solvent molecule plays an important role in forming favorable solvent-protein contacts.

The PMFs from MD simulations and 3D-RISM presented here correspond to, strictly speaking, different reaction coordinates and solute concentrations. In addition, the 3D-RISM results could in principle depend on the applied closure relation and additional parameters. Moreover, 3D-RISM calculations require nonzero LJ interactions to ensure convergence, whereas many force fields for MD simulation do not apply LJ interactions to hydrogen atoms. We therefore tested carefully whether any of these factors could account for the large discrepancies between the MD-based and 3D-RISM-based PMFs for nonwater solutes (Figure 3), as follows:

- **RISM Parameters.** We tested the influence of the water model, grid spacing, and tolerances used during RISM calculations. Changing these parameters had only small effects on the PMFs presented here. However, we recommend to carefully test the effect of the grid spacing, which had a minor influence on the PMFs in some test calculations (Figures S2).

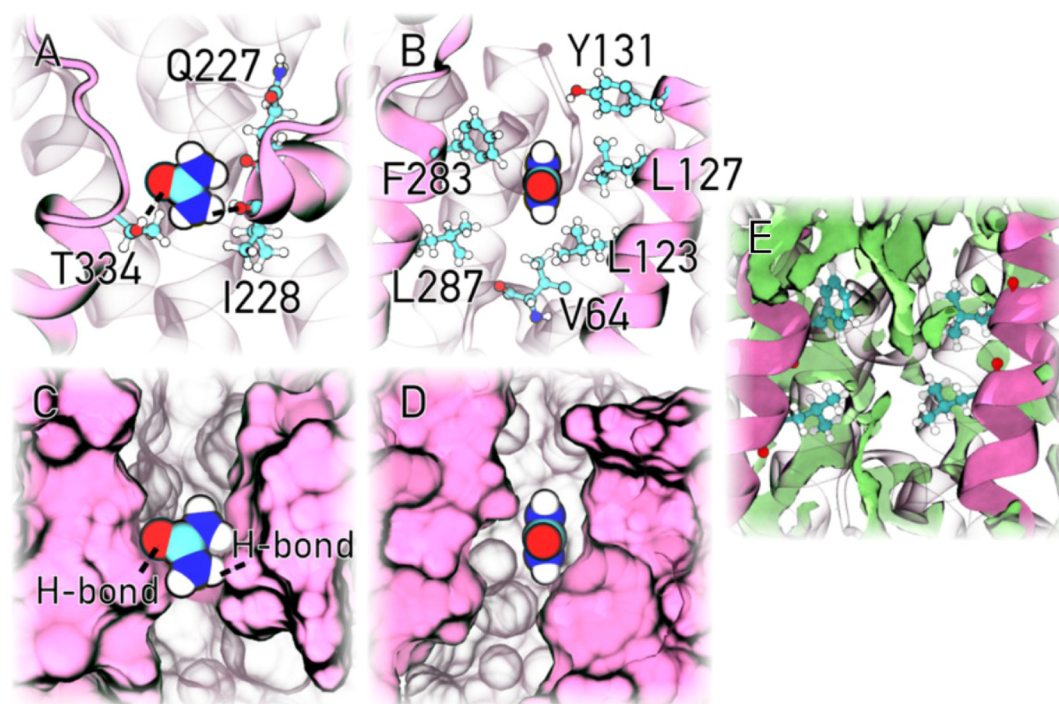


Figure 7. Urea binding site in UT-B S_0 region. The protein is visualized in pink/white cartoon representation (A, B, F) or as surface (C, D). Urea is shown as spheres, and some side chains as ball-and-stick. The color coding for the atoms is as follows: carbon (turquoise), oxygen (red), nitrogen (blue), and hydrogen (white). The snapshots were taken from US MD simulations. (A, C) Hydrogen bonds formed between the urea oxygen and T334 hydrogen, as well as between a urea hydrogen and I228 oxygen are depicted as black dashed lines. (B, D) 90 deg rotation of part A, illustrating favorable apolar contacts between urea and apolar residues F283, L287, L123, and L127. (E) 3D density of the urea carbon from 3D-RISM. The green isosurface indicates $g(r) > 2$.

- **Solute Concentration.** The MD-based PMFs represent the permeation of a single solute, whereas the 3D-RISM calculations yield densities at a given finite concentration of the permeating solute. Hence, we carried out RISM calculation at various concentrations of the nonwater permeating solute. Varying the concentration had only a marginal effect on the PMFs, suggesting that the different concentrations in MD simulations and 3D-RISM calculations (single-solute vs specific concentration, respectively) does not account for the observed discrepancies (Figure 3).
- **Reaction Coordinate.** In this study, the reaction coordinate used for most MD-based PMFs was defined via the center of mass of the permeating solute, as used in many previous MD studies, whereas the PMFs from 3D-RISM were computed from the density of one specific atom of the permeating solute. In other words, the definition of the reaction coordinate slightly differs between the MD-based and 3D-RISM-based PMFs. However, since the maximum distance between the solute's center of mass and the solvent site used to compute the 3D-RISM PMFs was only 0.73 Å, a larger artifact on the PMF seems unlikely. To further exclude that the slightly different reaction coordinates account for the observed discrepancies (Figure 3), we recomputed the PMF for urea permeation across UT-B using the position of the urea carbon atom as reaction coordinate instead of the urea center of mass (Figure S3). As expected, the PMF hardly depends on the details of the reaction coordinate (center of mass vs carbon position). In addition, we recomputed the 3D-RISM PMFs from the density of different atomic sites (Figure 8). We found that the 3D-RISM PMFs strongly depend on the solvent site purely for urea and methanol at the narrow ar/R region of aquaporin, where 3D-RISM predicts a tiny solvent density (Figure 8G,H, $z \approx 0.75$ nm). Here, purely for steric reasons, atoms near the molecule's rim may penetrate the constriction site more easily as compared to atoms near the center of the molecule leading to a reduced peak height. In contrast, all PMFs along the UT-B pore and PMFs for aquaporin outside the ar/R region hardly depend on the solvent site used to compute the PMF. For instance, none of the 3D-RISM-based urea PMFs exhibit a binding site in UT-B, irrespective of the atomic site (Figure 8C). These analyses demonstrate that the large discrepancies between the MD-based PMFs and the 3D-RISM-based PMFs are not due to slightly different reaction coordinates, but instead due to differences in the spatial distribution of the entire permeating solute.
- **Closure Relation.** We used the hypernetted-chain equation (HNC) and the partial series expansion of order- n (PSE $_n$) closure relations instead of the KH closure relation to converge the DRISM and 3D-RISM solutions. However, RISM calculations with HNC and PSE $_n$ suffered from poorer convergence,^{68,113} forcing us to increase the tolerance setting to achieve convergence in some cases (Tables S1 and S2). If the calculations converged, the results were similar to calculations with the KH closure in many cases (Figures 6 and S1). A notable exception are the PMFs for ammonia and water for AQP1, which exhibit a spuriously high peak at the ar/

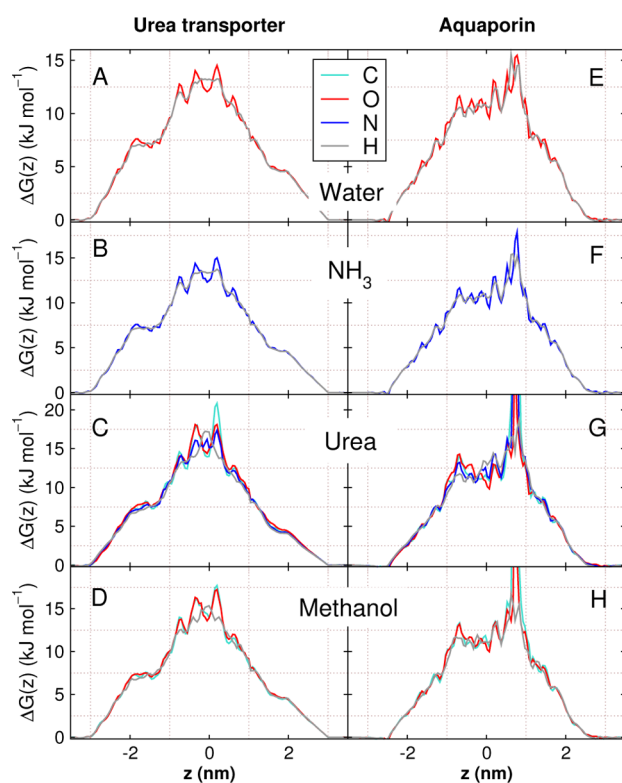


Figure 8. Water, NH_3 , urea, and methanol PMFs $\Delta G(z)$ calculated with 3D-RISM across UT-B channel (left) and AQP1 (right) based on the density of different solute atomic sites, as encoded by the line color (see legend: C, carbon atom; H, hydrogen; O, oxygen; N, nitrogen). Varying the solvent site has only a small effect on the overall PMFs. An exception is observed at the high peak at the ar/R site of AQP1 for urea and methanol (G, H). Here, atoms near the molecule's rim may penetrate the constriction site more easily as compared to atoms near the center of the molecule, leading to a different peak shapes.

R region, suggesting that the 3D-RISM with chained $\text{PSE}_1/\text{PSE}_2/\text{PSE}_3$ closures underestimate the ammonia and water densities at the ar/R site. Hence, the PSE closures do not provide an advantage over the KH closure for the systems considered here, either due to poorer convergence properties or due to problems in the narrow ar/R site of AQP1.

- LJ Parameters on Hydrogen Atoms.** We recomputed the PMF for urea across UT-B using a urea topology with nonzero LJ interactions on the hydrogen atoms, as also used during 3D-RISM calculations. However, LJ interactions on the hydrogen atoms had only a small effect on the PMFs (Figure S3). Hence LJ interactions of the hydrogen atoms (typically absent during MD, present during RISM) do not account for the different urea PMFs from MD and 3D-RISM.

Taken together, none of these parameters may explain the discrepancies between the MD-based and the RISM-based PMFs for nonwater solutes.

Furthermore, we investigated the possibility of computing the PMFs for the permeation of nonwater molecules based on hydration free energy predictions by 3D-RISM. Accordingly, we defined the protein and the permeating molecule as the 3D-RISM solute and purely water as the 3D-RISM solvent. Next, we computed the hydration free energy ΔG_{hyd} of the 3D-RISM solute (protein plus permeating molecule) as a function of

solute position along the channel, and we averaged the calculation over many conformations of the permeating molecule. However, the calculated PMF converged poorly because the ΔG_{hyd} values heavily fluctuated as a function of solute position and orientation, even if the protein coordinates were frozen. Hence, PMF calculations based on hydration free energy calculations do not provide a useful alternative to calculations with solvent mixtures.

The 3D-RISM PMFs reported here for AQP1 strongly differ from the profiles reported by Phongphanphanee *et al.*,⁴¹ which requires some explanation. For instance, our water PMFs exhibit barriers of at least 10 kJ mol^{-1} , whereas the water profiles reported by Phongphanphanee *et al.* are essentially flat. As discussed previously,⁵³ the barriers of 10 to 12 kJ mol^{-1} do not imply an empty channel, but merely reflect the entropic penalty due to the narrowing of the channel as compared to bulk water. As shown above, our PMFs imply that AQP1 and UT-B are filled by water (Table 1). The profiles reported by Phongphanphanee *et al.* are flat because the authors divided the 1D-density by the cross section area of the pore (eq 4 in ref 40) before translating the 1D-density into a PMF. Hence, the 1D-density does not correspond to the density of states of the solute along the reaction coordinate z , but instead to the solute density only *inside* the pore. Consequently, the profiles reported by Phongphanphanee *et al.* are not PMFs and cannot be compared to the PMFs reported here. However, we speculate that the profiles in ref 41 would resemble the PMFs presented here if they are corrected by the entropic cost due to narrowing of the pore $\Delta S_{\text{pore}}(z) = k_B \ln(A_{\text{pore}}(z)/A_{\text{mono}})$, where $A_{\text{pore}}(z)$ denotes the cross section area of the pore.

CONCLUSIONS

3D-RISM allows computationally highly efficient calculations of PMFs for water permeation across membrane channels at reasonable accuracy. In the case of UT-B, the water density inside the narrowest channel lumen predicted by 3D-RISM was $\sim 50\%$ lower as compared to the water density suggested by MD simulations, corresponding to differences of $\sim 2 \text{ kJ mol}^{-1}$ in the PMFs. For AQP1, we found nearly quantitative agreement between 3D-RISM and MD simulations. Hence, the computationally cheap 3D-RISM method provides an attractive alternative to MD simulation for such applications. However, for PMFs of nonwater permeation, which require the treatment of solvent mixtures, we found large discrepancies between 3D-RISM and MD, even if the structural fluctuations of the protein were taken into account during 3D-RISM calculations. We speculated that these discrepancies might reflect (i) inaccurate treatment of hydrophobic effects in 3D-RISM and (ii) limitations due to the orientational averages inherent to current RISM methods. We hope that our study provides a starting point for future developments of RISM-based methods.

APPENDIX: ENTROPY IN A FLAT-BOTTOMED CYLINDRICAL POTENTIAL

During US simulations, the solutes were restrained to a cylinder by a cylindrical flat-bottomed potential $V_{\text{cyl}}(r) = k_c(r - r_c)^2/2 \cdot H(r - r_c)$ (see Computational Details). The cross section area of the cylinder defines the area in which the solutes may laterally diffuse when the solute is in the bulk, far away from the channel. Hence, the PMF corresponds to a density of channels of one channel per cross section area A_{cyl} of the cylinder. Alternatively, the cylinder area may be considered as the bulk

reference area of the PMF. To translate the PMF to a new reference area A_{ref} (corresponding to a new density of channels $1/A_{\text{ref}}$), the PMF must be corrected for the change in entropy of the bulk upon changing the reference area from A_{cyl} to A_{ref} . That change of entropy is given by $\Delta S = k_B \ln(A_{\text{ref}}/A_{\text{cyl}})$. For a hard-core cylinder, the cylinder area would be simply $A_{\text{cyl}}^{\text{hc}} = \pi r_c^2$.

For a “soft” cylinder, in contrast, the entropy of the solute density defined by the flat-bottomed potential must be computed. The solute density is

$$\rho_{\text{cyl}}(r) = N^{-1} \begin{cases} 1 & \text{if } r \leq r_c, \\ \exp\left(-\frac{(r-r_c)^2}{2\sigma_c^2}\right) & \text{if } r > r_c. \end{cases} \quad (8)$$

Here, $\sigma_c = (k_B T/k_c)^{1/2}$ is the width of the Gaussian-shaped decay of the density in the quadratic region of the flat-bottomed potential. The normalization constant is

$$N = \pi(r_c^2 + 2\sigma_c^2 + \sqrt{2\pi}r_c\sigma_c) \quad (9)$$

such that $\rho_{\text{cyl}}(r)$ is normalized, $\int_0^\infty 2\pi r \rho_{\text{cyl}}(r) dr = 1$. The Shannon entropy of the distribution is

$$S_{\text{cyl}}[\rho_{\text{cyl}}] = -k_B \int_0^\infty 2\pi r \rho_{\text{cyl}}(r) \ln \rho_{\text{cyl}}(r) dr \quad (10)$$

$$= k_B \pi r_c^2 N^{-1} \ln N + 2k_B \pi \sigma_c N^{-1} [\sigma_c(1 + \ln N) + r_c \sqrt{\pi/2} (1/2 + \ln N)] \quad (11)$$

The Shannon entropy of a uniform distribution over the new reference area is $S_{\text{ref}} = k_B \ln A_{\text{ref}}$. Hence, the required correction in the bulk free energy is given by

$$\Delta G_{\text{bulk}} = -T(S_{\text{ref}} - S_{\text{cyl}}) \quad (12)$$

where T is the temperature. Because the free energy of the bulk state is often defined to zero, it is convenient to correct the region of the PMF corresponding to the inside of the channel by $-\Delta G_{\text{bulk}}$ instead of correcting the bulk region by ΔG_{bulk} .

As a numerical example, take $r_c = 0.7$ nm, $k_c = 500$ kJ mol⁻¹nm⁻², $T = 300$ K, and $A_{\text{ref}} = 10.3$ nm², corresponding to the cross section area of an aquaporin monomer.⁵² Then, we get $\Delta G_{\text{bulk}} = 3.851$ kJ/mol. Notably, approximating the cylinder area as $A_{\text{cyl}} = \pi(r_c + 2\sigma_c)^2$ yields a correction of 3.824 kJ mol⁻¹, in good agreement with the analytic result, as suggested previously.²¹ In contrast, neglecting the density outside of the flat region of the flat-bottomed potential ($A_{\text{cyl}} = \pi r_c^2$) would lead to an inaccurate correction of 4.74 kJ/mol.

■ ASSOCIATED CONTENT

● Supporting Information

The Supporting Information is available free of charge on the ACS Publications website at DOI: 10.1021/acs.jpcc.6b11279.

Additional details on DRISM and 3D-RISM calculations, as well as three figures that analyze the influence of (a) the closure relation, (b) the RISM grid spacing, (c) the reaction coordinate (based on solute center of mass versus central atom), and (d) of nonzero Lennard-Jones interactions of hydrogen atoms (PDF)

■ AUTHOR INFORMATION

Corresponding Author

* (J.S.H.) E-mail: jhub@gwdg.de. Telephone: +49-551-39-14189. Fax: +49-551-39-14082.

ORCID

Jochen S. Hub: 0000-0001-7716-1767

Notes

The authors declare no competing financial interest.

■ ACKNOWLEDGMENTS

We thank Stefan Kast for helpful discussions, and Kalina Atkovska for critically reading the manuscript. This study was supported by the Deutsche Forschungsgemeinschaft (HU 1971-1/1 and SFB 803/A12).

■ REFERENCES

- (1) Roux, B. The calculation of the potential of mean force using computer simulations. *Comput. Phys. Commun.* **1995**, *91*, 275–282.
- (2) Allen, T. W.; Andersen, O. S.; Roux, B. Molecular dynamics - potential of mean force calculations as a tool for understanding ion permeation and selectivity in narrow channels. *Biophys. Chem.* **2006**, *124*, 251–67.
- (3) Szabo, A.; Schulten, K.; Schulten, Z. First passage time approach to diffusion controlled reactions. *J. Chem. Phys.* **1980**, *72*, 4350–4357.
- (4) Woolf, T. B.; Roux, B. Molecular dynamics simulation of the gramicidin channel in a phospholipid bilayer. *Proc. Natl. Acad. Sci. U. S. A.* **1994**, *91*, 11631–11635.
- (5) Allen, T. W.; Andersen, O. S.; Roux, B. Energetics of ion conduction through the gramicidin channel. *Proc. Natl. Acad. Sci. U. S. A.* **2004**, *101*, 117–122.
- (6) Berneche, S.; Roux, B. Energetics of ion conduction through the K⁺ channel. *Nature* **2001**, *414*, 73–77.
- (7) Zhang, Y.; Voth, G. A. Combined metadynamics and umbrella sampling method for the calculation of ion permeation free energy profiles. *J. Chem. Theory Comput.* **2011**, *7*, 2277–2283.
- (8) Beckstein, O.; Sansom, M. S. A hydrophobic gate in an ion channel: the closed state of the nicotinic acetylcholine receptor. *Phys. Biol.* **2006**, *3*, 147.
- (9) Beckstein, O.; Tai, K.; Sansom, M. S. Not ions alone: barriers to ion permeation in nanopores and channels. *J. Am. Chem. Soc.* **2004**, *126*, 14694–14695.
- (10) Pongprayoon, P.; Beckstein, O.; Wee, C. L.; Sansom, M. S. Simulations of anion transport through OprP reveal the molecular basis for high affinity and selectivity for phosphate. *Proc. Natl. Acad. Sci. U. S. A.* **2009**, *106*, 21614–21618.
- (11) Chen, H.; Wu, Y.; Voth, G. A. Origins of proton transport behavior from selectivity domain mutations of the aquaporin-1 channel. *Biophys. J.* **2006**, *90*, L73–L75.
- (12) Pomès, R.; Roux, B. Molecular mechanism of H⁺ conduction in the single-file water chain of the gramicidin channel. *Biophys. J.* **2002**, *82*, 2304–2316.
- (13) Chakrabarti, N.; Tajkhorshid, E.; Roux, B.; Pomès, R. Molecular basis of proton blockage in aquaporins. *Structure* **2004**, *12*, 65–74.
- (14) Hummer, G.; Rasaiah, J. C.; Noworyta, J. P. Water conduction through the hydrophobic channel of a carbon nanotube. *Nature* **2001**, *414*, 188–190.
- (15) De Groot, B. L.; Frigato, T.; Helms, V.; Grubmüller, H. The mechanism of proton exclusion in the aquaporin-1 water channel. *J. Mol. Biol.* **2003**, *333*, 279–293.
- (16) de Groot, B. L.; Grubmüller, H. Water permeation across biological membranes: mechanism and dynamics of aquaporin-1 and GlpF. *Science* **2001**, *294*, 2353–2357.
- (17) Tajkhorshid, E.; Nollert, P.; Jensen, M. Ø.; Miercke, L. J.; O’Connell, J.; Stroud, R. M.; Schulten, K. Control of the selectivity of the aquaporin water channel family by global orientational tuning. *Science* **2002**, *296*, 525–530.

- (18) Hub, J. S.; de Groot, B. L. Does CO₂ permeate through aquaporin-1? *Biophys. J.* **2006**, *91*, 842–848.
- (19) Müller, E. M.; Hub, J. S.; Grubmüller, H.; de Groot, B. L. Is TEA an inhibitor for human Aquaporin-1? *Pfluegers Arch.* **2008**, *456*, 663–669.
- (20) Portella, G.; Hub, J. S.; Vesper, M. D.; De Groot, B. L. Not only enthalpy: large entropy contribution to ion permeation barriers in single-file channels. *Biophys. J.* **2008**, *95*, 2275–2282.
- (21) Hub, J. S.; Winkler, F. K.; Merrick, M.; de Groot, B. L. Potentials of mean force and permeabilities for carbon dioxide, ammonia, and water flux across a Rhesus protein channel and lipid membranes. *J. Am. Chem. Soc.* **2010**, *132*, 13251–13263.
- (22) Kästner, J. Umbrella sampling. *Wiley Interdiscip. Rev. Comput. Mol. Sci.* **2011**, *1*, 932–942.
- (23) Baştuğ, T.; Kuyucak, S. Free energy simulations of single and double ion occupancy in gramicidin A. *J. Chem. Phys.* **2007**, *126*, 105103.
- (24) Allen, T. W.; Andersen, O. S.; Roux, B. Ion permeation through a narrow channel: using gramicidin to ascertain all-atom molecular dynamics potential of mean force methodology and biomolecular force fields. *Biophys. J.* **2006**, *90*, 3447–3468.
- (25) Hirata, F. In *Molecular Theory of Solvation (Understanding Chemical Reactivity)*; Hirata, F., Ed.; Kluwer Academic Publishers: Dordrecht, The Netherlands, 2004; Vol. 24.
- (26) Beglov, D.; Roux, B. An integral equation to describe the solvation of polar molecules in liquid water. *J. Phys. Chem. B* **1997**, *101*, 7821–7826.
- (27) Kovalenko, A.; Hirata, F. Three-dimensional density profiles of water in contact with a solute of arbitrary shape: a RISM approach. *Chem. Phys. Lett.* **1998**, *290*, 237–244.
- (28) Stumpe, M. C.; Blinov, N.; Wishart, D.; Kovalenko, A.; Pande, V. S. Calculation of local water densities in biological systems: a comparison of molecular dynamics simulations and the 3D-RISM-KH molecular theory of solvation. *J. Phys. Chem. B* **2011**, *115*, 319–28.
- (29) Imai, T.; Harano, Y.; Kinoshita, M.; Kovalenko, A.; Hirata, F. A theoretical analysis on hydration thermodynamics of proteins. *J. Chem. Phys.* **2006**, *125*, 024911.
- (30) Imai, T.; Oda, K.; Kovalenko, A.; Hirata, F.; Kidera, A. Ligand mapping on protein surfaces by the 3D-RISM theory: Toward computational fragment-based drug design. *J. Am. Chem. Soc.* **2009**, *131*, 12430–12440.
- (31) Pettitt, B. M.; Rossky, P. J. Integral equation predictions of liquid state structure for waterlike intermolecular potentials. *J. Chem. Phys.* **1982**, *77*, 1451–1457.
- (32) Beglov, D.; Roux, B. Solvation of complex molecules in a polar liquid: an integral equation theory. *J. Chem. Phys.* **1996**, *104*, 8678–8689.
- (33) Huang, W.; Blinov, N.; Wishart, D. S.; Kovalenko, A. Role of Water in Ligand Binding to Maltose-Binding Protein: Insight from a New Docking Protocol Based on the 3D-RISM-KH Molecular Theory of Solvation. *J. Chem. Inf. Model.* **2015**, *55*, 317–328.
- (34) Palmer, D. S.; Frolov, A. I.; Ratkova, E. L.; Fedorov, M. V. Towards a universal method for calculating hydration free energies: a 3D reference interaction site model with partial molar volume correction. *J. Phys.: Condens. Matter* **2010**, *22*, 492101.
- (35) Joung, I. S.; Luchko, T.; Case, D. a. Simple electrolyte solutions: Comparison of DRISM and molecular dynamics results for alkali halide solutions. *J. Chem. Phys.* **2013**, *138*, 044103.
- (36) Imai, T.; Hiraoka, R.; Kovalenko, A.; Hirata, F. Water molecules in a protein cavity detected by a statistical-mechanical theory. *J. Am. Chem. Soc.* **2005**, *127*, 15334–15335.
- (37) Imai, T.; Kovalenko, A.; Hirata, F. Hydration structure, thermodynamics, and functions of protein studied by the 3D-RISM theory. *Mol. Simul.* **2006**, *32*, 817–824.
- (38) Kovalenko, A.; Kobryn, A. E.; Gusarov, S.; Lyubimova, O.; Liu, X.; Blinov, N.; Yoshida, M. Molecular theory of solvation for supramolecules and soft matter structures: application to ligand binding, ion channels, and oligomeric polyelectrolyte gels. *Soft Matter* **2012**, *8*, 1508.
- (39) Phongphanphanee, S.; Yoshida, N.; Hirata, F. The statistical-mechanics study for the distribution of water molecules in aquaporin. *Chem. Phys. Lett.* **2007**, *449*, 196–201.
- (40) Phongphanphanee, S.; Yoshida, N.; Hirata, F. The potential of mean force of water and ions in aquaporin channels investigated by the 3D-RISM method. *J. Mol. Liq.* **2009**, *147*, 107–111.
- (41) Phongphanphanee, S.; Yoshida, N.; Hirata, F. Molecular selectivity in aquaporin channels studied by the 3D-RISM theory. *J. Phys. Chem. B* **2010**, *114*, 7967–73.
- (42) Huang, W.; Blinov, N.; Kovalenko, A. Octanol-Water Partition Coefficient from 3D-RISM-KH Molecular Theory of Solvation with Partial Molar Volume Correction. *J. Phys. Chem. B* **2015**, *119*, 5588–5597.
- (43) Cao, S.; Sheong, F. K.; Huang, X. Reference interaction site model with hydrophobicity induced density inhomogeneity: An analytical theory to compute solvation properties of large hydrophobic solutes in the mixture of polyatomic solvent molecules. *J. Chem. Phys.* **2015**, *143*, 054110.
- (44) Luchko, T.; Gusarov, S.; Roe, D. R.; Simmerling, C.; Case, D. a.; Tuszynski, J.; Kovalenko, A. Three-dimensional molecular theory of solvation coupled with molecular dynamics in Amber. *J. Chem. Theory Comput.* **2010**, *6*, 607–624.
- (45) Howard, J. J.; Pettitt, B. M. Integral Equations in the Study of Polar and Ionic Interaction Site Fluids. *J. Stat. Phys.* **2011**, *145*, 441–466.
- (46) Fedotova, M. V.; Dmitrieva, O. a. Ion-selective interactions of biologically relevant inorganic ions with alanine zwitterion: a 3D-RISM study. *Amino Acids* **2015**, *47*, 1015–1023.
- (47) Heil, J.; Kast, S. M. 3D RISM theory with fast reciprocal-space electrostatics. *J. Chem. Phys.* **2015**, *142*, 114107.
- (48) Tanwar, A. S.; Sindhikara, D. J.; Hirata, F.; Anand, R. Determination of the Formylglycinamide Ribonucleotide Amidotransferase Ammonia Pathway by Combining 3D-RISM Theory with Experiment. *ACS Chem. Biol.* **2015**, *10*, 698–704.
- (49) Thiel, G.; Baumeister, D.; Schroeder, I.; Kast, S. M.; Van Etten, J. L.; Moroni, A. Minimal art: or why small viral K⁺ channels are good tools for understanding basic structure and function relations. *Biochim. Biophys. Acta, Biomembr.* **2011**, *1808*, 580–588.
- (50) Tayefeh, S.; Kloss, T.; Kreim, M.; Gebhardt, M.; Baumeister, D.; Hertel, B.; Richter, C.; Schwalbe, H.; Moroni, A.; Thiel, G.; et al. Model development for the viral Kcv potassium channel. *Biophys. J.* **2009**, *96*, 485–498.
- (51) Kast, S. M.; Kloss, T.; Tayefeh, S.; Thiel, G. A minimalist model for ion partitioning and competition in a K⁺ channel selectivity filter. *J. Gen. Physiol.* **2011**, *138*, 371–373.
- (52) Hub, J. S.; de Groot, B. L. Mechanism of selectivity in aquaporins and aquaglyceroporins. *Proc. Natl. Acad. Sci. U. S. A.* **2008**, *105*, 1198–1203.
- (53) Hub, J. S.; de Groot, B. L. Comment on “Molecular selectivity in aquaporin channels studied by the 3D-RISM theory”. *J. Phys. Chem. B* **2011**, *115*, 8364–8366.
- (54) Phongphanphanee, S.; Yoshida, N.; Hirata, F. Reply to “Comment on ‘Molecular Selectivity in Aquaporin Channels Studied by the 3D-RISM Theory’”. *J. Phys. Chem. B* **2011**, *115*, 8367.
- (55) Yang, B.; Sands, M. J. *Urea Transporters*; Springer Netherlands: Dordrecht, The Netherlands, 2014.
- (56) Smith, C. P. Mammalian urea transporters. *Exp. Physiol.* **2009**, *94*, 180–185.
- (57) Levin, E. J.; Cao, Y.; Enkavi, G.; Quick, M.; Pan, Y.; Tajkhorshid, E.; Zhou, M. Structure and permeation mechanism of a mammalian urea transporter. *Proc. Natl. Acad. Sci. U. S. A.* **2012**, *109*, 11194–9.
- (58) Zhao, D.; Sonawane, N.; Levin, M. H.; Yang, B. Comparative transport efficiencies of urea analogues through urea transporter UT-B. *Biochim. Biophys. Acta, Biomembr.* **2007**, *1768*, 1815–1821.
- (59) Geyer, R. R.; Musa-Aziz, R.; Enkavi, G.; Mahinthichaichan, P.; Tajkhorshid, E.; Boron, W. F. Movement of NH through the human urea transporter B: a new gas channel. *Am. J. Physiol. Renal Physiol.* **2013**, *304*, F1447–57.

- (60) Azouzi, S.; Gueroult, M.; Ripoché, P.; Genetet, S.; Colin Aronovicz, Y.; Le Van Kim, C.; Etchebest, C.; Mouro-Chanteloup, I. Energetic and Molecular Water Permeation Mechanisms of the Human Red Blood Cell Urea Transporter B. *PLoS One* **2013**, *8*, e82338.
- (61) Yang, B.; Verkman, A. S. Analysis of Double Knockout Mice Lacking Aquaporin-1 and Urea Transporter UT-B: EVIDENCE FOR UT-B-FACILITATED WATER TRANSPORT IN ERYTHROCYTES. *J. Biol. Chem.* **2002**, *277*, 36782–36786.
- (62) Preston, G. M.; Carroll, T. P.; Guggino, W. B.; Agre, P. Appearance of water channels in *Xenopus* oocytes expressing red cell CHIP28 protein. *Science* **1992**, *256*, 385–387.
- (63) Gomes, D.; Agasse, A.; Thiébaud, P.; Delrot, S.; Gerós, H.; Chaumont, F. Aquaporins are multifunctional water and solute transporters highly divergent in living organisms. *Biochim. Biophys. Acta, Biomembr.* **2009**, *1788*, 1213–1228.
- (64) Murata, K.; Mitsuoka, K.; Hirai, T.; Walz, T.; Agre, P.; Heymann, J. B.; Engel, A.; Fujiyoshi, Y. Structural determinants of water permeation through aquaporin-1. *Nature* **2000**, *407*, 599–605.
- (65) Sui, H.; Han, B.-G.; Lee, J. K.; Walian, P.; Jap, B. K. Structural basis of water-specific transport through the AQP1 water channel. *Nature* **2001**, *414*, 872–878.
- (66) Holm, L. M.; Jahn, T. P.; Möller, A. L.; Schjoerring, J. K.; Ferri, D.; Klaerke, D. A.; Zeuthen, T. NH₃ and NH₄⁺ permeability in aquaporin-expressing *Xenopus* oocytes. *Pfluegers Arch.* **2005**, *450*, 415–428.
- (67) Beitz, E.; Wu, B.; Holm, L. M.; Schultz, J. E.; Zeuthen, T. Point mutations in the aromatic/arginine region in aquaporin 1 allow passage of urea, glycerol, ammonia, and protons. *Proc. Natl. Acad. Sci. U. S. A.* **2006**, *103*, 269–274.
- (68) Hansen, J.-P.; McDonald, I. R. *Theory of Simple Liquids: With Applications to Soft Matter*; Academic Press: 2013.
- (69) Frenkel, D.; Smit, B. *Understanding molecular simulation: from algorithms to applications*; Academic press: 2001; Vol. 1.
- (70) Torrie, G. M.; Valleau, J. P. Monte Carlo free energy estimates using non-Boltzmann sampling: application to the sub-critical Lennard-Jones fluid. *Chem. Phys. Lett.* **1974**, *28*, 578–581.
- (71) Kumar, S.; Rosenberg, J. M.; Bouzida, D.; Swendsen, R. H.; Kollman, P. A. The weighted histogram analysis method for free-energy calculations on biomolecules. I. The method. *J. Comput. Chem.* **1992**, *13*, 1011–1021.
- (72) Perkyns, J.; Pettitt, B. M. A site–site theory for finite concentration saline solutions. *J. Chem. Phys.* **1992**, *97*, 7656–7666.
- (73) Perkyns, J.; Pettitt, B. M. A dielectrically consistent interaction site theory for solvent–electrolyte mixtures. *Chem. Phys. Lett.* **1992**, *190*, 626–630.
- (74) Baxter, R. Ornstein–Zernike relation and Percus–Yevick approximation for fluid mixtures. *J. Chem. Phys.* **1970**, *52*, 4559–4562.
- (75) Waisman, E.; Lebowitz, J. L. Mean spherical model integral equation for charged hard spheres I. Method of solution. *J. Chem. Phys.* **1972**, *56*, 3086–3093.
- (76) Kovalenko, A.; Hirata, F. Self-consistent description of a metal–water interface by the Kohn–Sham density functional theory and the three-dimensional reference interaction site model. *J. Chem. Phys.* **1999**, *110*, 10095–10112.
- (77) Wolf, M. G.; Hoefling, M.; Aponte-Santamaría, C.; Grubmüller, H.; Groenhof, G. g_membed: Efficient insertion of a membrane protein into an equilibrated lipid bilayer with minimal perturbation. *J. Comput. Chem.* **2010**, *31*, 2169–2174.
- (78) Jorgensen, W. L.; Chandrasekhar, J.; Madura, J. D.; Impey, R. W.; Klein, M. L. Comparison of simple potential functions for simulating liquid water. *J. Chem. Phys.* **1983**, *79*, 926–935.
- (79) Lindorff-Larsen, K.; Piana, S.; Palmo, K.; Maragakis, P.; Klepeis, J. L.; Dror, R. O.; Shaw, D. E. Improved side-chain torsion potentials for the Amber ff99SB protein force field. *Proteins Struct. Funct. Bioinform.* **2010**, *78*, 1950–1958.
- (80) Berger, O.; Edholm, O.; Jähnig, F. Molecular dynamics simulations of a fluid bilayer of dipalmitoylphosphatidylcholine at full hydration, constant pressure, and constant temperature. *Biophys. J.* **1997**, *72*, 2002.
- (81) Cordero, A.; Caltabiano, G.; Pardo, L. Membrane protein simulations using AMBER force field and Berger lipid parameters. *J. Chem. Theory Comput.* **2012**, *8*, 948–958.
- (82) Pronk, S.; Páll, S.; Schulz, R.; Larsson, P.; Bjelkmar, P.; Apostolov, R.; Shirts, M. R.; Smith, J. C.; Kasson, P. M.; Van Der Spoel, D.; et al. GROMACS 4.5: A high-throughput and highly parallel open source molecular simulation toolkit. *Bioinformatics* **2013**, *29*, 845–854.
- (83) Essmann, U.; Perera, L.; Berkowitz, M. L.; Darden, T.; Lee, H.; Pedersen, L. G. A smooth particle mesh Ewald method. *J. Chem. Phys.* **1995**, *103*, 8577.
- (84) Miyamoto, S.; Kollman, P. A. SETTLE: an analytical version of the SHAKE and RATTLE algorithm for rigid water models. *J. Comput. Chem.* **1992**, *13*, 952–962.
- (85) Hess, B. P-LINCS: A parallel linear constraint solver for molecular simulation. *J. Chem. Theory Comput.* **2008**, *4*, 116–122.
- (86) Feenstra, K. A.; Hess, B.; Berendsen, H. J. Improving efficiency of large timescale molecular dynamics simulations of hydrogen-rich systems. *J. Comput. Chem.* **1999**, *20*, 786–798.
- (87) Bussi, G.; Donadio, D.; Parrinello, M. Canonical sampling through velocity rescaling. *J. Chem. Phys.* **2007**, *126*, 014101.
- (88) Berendsen, H. J.; Postma, J. v.; van Gunsteren, W. F.; DiNola, A.; Haak, J. Molecular dynamics with coupling to an external bath. *J. Chem. Phys.* **1984**, *81*, 3684–3690.
- (89) Salomon-Ferrer, R.; Case, D. A.; Walker, R. C. An overview of the Amber biomolecular simulation package. *Wiley Interdiscip. Rev. Comput. Mol. Sci.* **2013**, *3*, 198–210.
- (90) Jakalian, A.; Bush, B. L.; Jack, D. B.; Bayly, C. I. Fast, efficient generation of high-quality atomic Charges. AM1-BCC model: I. Method. *J. Comput. Chem.* **2000**, *21*, 132–146.
- (91) Jakalian, A.; Jack, D. B.; Bayly, C. I. Fast, efficient generation of high-quality atomic charges. AM1-BCC model: II. Parameterization and validation. *J. Comput. Chem.* **2002**, *23*, 1623–1641.
- (92) Jorgensen, W. L.; Maxwell, D. S.; Tirado-Rives, J. Development and testing of the OPLS all-atom force field on conformational energetics and properties of organic liquids. *J. Am. Chem. Soc.* **1996**, *118*, 11225–11236.
- (93) Kaminski, G. A.; Friesner, R. A.; Tirado-Rives, J.; Jorgensen, W. L. Evaluation and reparameterization of the OPLS-AA force field for proteins via comparison with accurate quantum chemical calculations on peptides. *J. Phys. Chem. B* **2001**, *105*, 6474–6487.
- (94) Duffy, E. M.; Severance, D. L.; Jorgensen, W. L. Urea: potential functions, log P, and free energy of hydration. *Isr. J. Chem.* **1993**, *33*, 323–330.
- (95) MacKerell, A. D. J.; Bashford, D.; Bellott, M.; Dunbrack, R. L.; Evanseck, J. D.; Field, M. J.; Fischer, S.; Gao, J.; Guo, H.; Ha, S.; et al. All-atom empirical potential for molecular modeling and dynamics studies of proteins. *J. Phys. Chem. B* **1998**, *102*, 3586–616.
- (96) Caleman, C.; van Maaren, P. J.; Hong, M.; Hub, J. S.; Costa, L. T.; van der Spoel, D. Force field benchmark of organic liquids: density, enthalpy of vaporization, heat capacities, surface tension, isothermal compressibility, volumetric expansion coefficient, and dielectric constant. *J. Chem. Theory Comput.* **2012**, *8*, 61–74.
- (97) van der Spoel, D.; van Maaren, P. J.; Caleman, C. GROMACS molecule & liquid database. *Bioinformatics* **2012**, *28*, 752–753.
- (98) Van Gunsteren, W.; Berendsen, H. A leap-frog algorithm for stochastic dynamics. *Mol. Simul.* **1988**, *1*, 173–185.
- (99) Parrinello, M.; Rahman, A. Polymorphic transitions in single crystals: A new molecular dynamics method. *J. Appl. Phys.* **1981**, *52*, 7182–7190.
- (100) Nosé, S.; Klein, M. L. Constant pressure molecular dynamics for molecular systems. *Mol. Phys.* **1983**, *50*, 1055–1076.
- (101) Hub, J. S.; De Groot, B. L.; Van Der Spoel, D. g_wham A Free Weighted Histogram Analysis Implementation Including Robust Error and Autocorrelation Estimates. *J. Chem. Theory Comput.* **2010**, *6*, 3713–3720.

(102) Cortis, C. M.; Rosky, P. J.; Friesner, R. A. A three-dimensional reduction of the Ornstein–Zernicke equation for molecular liquids. *J. Chem. Phys.* **1997**, *107*, 6400–6414.

(103) Du, Q.; Beglov, D.; Roux, B. Solvation free energy of polar and nonpolar molecules in water: an extended interaction site integral equation theory in three dimensions. *J. Phys. Chem. B* **2000**, *104*, 796–805.

(104) Kovalenko, A.; Hirata, F. Hydration free energy of hydrophobic solutes studied by a reference interaction site model with a repulsive bridge correction and a thermodynamic perturbation method. *J. Chem. Phys.* **2000**, *113*, 2793–2805.

(105) Gusarov, S.; Pujari, B. S.; Kovalenko, A. Efficient treatment of solvation shells in 3D molecular theory of solvation. *J. Comput. Chem.* **2012**, *33*, 1478–1494.

(106) Giambaşu, G. M.; Luchko, T.; Herschlag, D.; York, D. M.; Case, D. A. Ion counting from explicit-solvent simulations and 3D-RISM. *Biophys. J.* **2014**, *106*, 883–894.

(107) Lee, P.-H.; Helms, V. Identifying continuous pores in protein structures with PROPORES by computational repositioning of gating residues. *Proteins: Struct., Funct., Genet.* **2012**, *80*, 421–432.

(108) Bankir, L.; Bouby, N.; Trinh-Trang-Tan, M.-M.; Ahloulay, M.; Promeneur, D. Direct and indirect cost of urea excretion. *Kidney Int.* **1996**, *49*, 1598–1607.

(109) Hashido, M.; Kidera, A.; Ikeguchi, M. Water transport in aquaporins: osmotic permeability matrix analysis of molecular dynamics simulations. *Biophys. J.* **2007**, *93*, 373–385.

(110) Nikolic, D.; Blinov, N.; Wishart, D.; Kovalenko, A. 3D-RISM-Dock: A new fragment-based drug design protocol. *J. Chem. Theory Comput.* **2012**, *8*, 3356–3372.

(111) Hub, J. S.; Grubmüller, H.; de Groot, B. L. Dynamics and energetics of permeation through aquaporins. What do we learn from molecular dynamics simulations? *Handb. Exp. Pharmacol.* **2009**, *190*, 57–76.

(112) Wang, Z.; Yu, T.; Sang, J.-P.; Zou, X.-W.; Yan, C.; Zou, X. Computation and Simulation of the Structural Characteristics of the Kidney Urea Transporter and Behaviors of Urea Transport. *J. Phys. Chem. B* **2015**, *119*, 5124–5131.

(113) Kast, S. M.; Kloss, T. Closed-form expressions of the chemical potential for integral equation closures with certain bridge functions. *J. Chem. Phys.* **2008**, *129*, 236101.